ACS APPLIED POLYMER MATERIALS

pubs.acs.org/acsapm Article

Recycling Commodity Plastic Waste for Vat Photopolymerization 3D Printing of High-Performance Polymeric Composites

Farzad Gholami, Mingzhe Li, Alvaro Hucker, Summer Clark, Frédéric Demoly, Kun Zhou, and Hang Jerry Qi*

Cite This: *ACS Appl. Polym. Mater.* 2025, 7, 16194−16205

Read Online

ACCESS | Metrics & More | Article Recommendations | Supporting Information

ABSTRACT: Recycling plastic waste is crucial for reducing environmental harm and conserving resources. However, current methods face challenges, such as the need to sort different polymers, limited compatibility across plastic types, and reliance on hazardous chemicals in chemical recycling. This study introduces a sustainable additive manufacturing approach by repurposing commonly discarded thermoplastics, including polylactic acid (PLA), polyamide (PA), polypropylene (PP), polyethylene terephthalate (PET), and 3D-printed thermosets, as feedstock for digital light processing (DLP) 3D printing. Using cryogenic milling, these polymers are transformed into fine powders and incorporated into a photocurable resin to create polymeric composites. The addition of solid plastic particles presents two main challenges: increased resin viscosity and UV light blocking. These issues affect both printability and mechanical performance. To address viscosity, a heated vat system maintains the resin at ∼55 °C, improving flow without compromising the process. Additionally, UV light is blocked during photopolymerization, leading to incomplete curing and a 50% reduction in modulus compared to neat resin. A dual-curing approach mitigates this by combining UV-curing via a photoinitiator with thermal annealing via a thermal initiator, ensuring full polymerization and restoring mechanical strength. This strategy yields an ∼250% increase in modulus for high-loading samples, aligning with theoretical predictions. The study demonstrates broad applicability across various powder−resin combinations, highlighting its adaptability in diverse material contexts. Overall, this work establishes a pathway for incorporating a wide range of recycled plastics into high-performance 3D-printed composites, advancing both the sustainability and the functional potential of additive manufacturing.

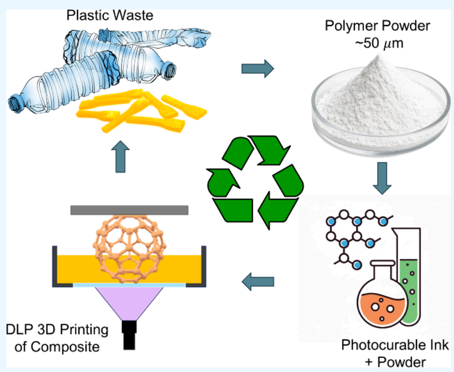

KEYWORDS: *Vat photopolymerization, Cryogenic milling, Polymeric composites, Digital light processing (DLP), Dual-curing, Recycled thermoplastics*

INTRODUCTION

Globally, plastic waste has reached alarming levels, with millions of tons being added to landfills every year.[1] Not only does plastic waste occupy significant landfill space and contaminate soil and water through the release of harmful chemicals as it breaks down, but its production and disposal also contribute to greenhouse gas emissions, further intensifying the global climate crisis.[2] Addressing these issues is imperative to mitigate the environmental impact of plastic pollution and ensure a sustainable future.

Additive manufacturing (AM), also known as 3D printing, is a very popular technique for the rapid creation of complex objects in a layer-by-layer method.[3−5] Compared to conventional manufacturing techniques, AM offers several advantages such as flexibility and design freedom, low-cost and efficient production, and applicability to a wide range of materials including polymers, ceramics, and metals.[6−8] 3D printing of polymers, due to the ease of use and affordability, is the most common and widely used in past decades at the industrial and research level.[9,10] While recently becoming widespread, like other production technologies, sustainability is a large concern in 3D printing. Nowadays, polymer 3D printers are available to purchase at a remarkably low cost (as low as several hundred US dollars), which makes them attractive for users to be able to print 3D objects at home for a hobby or their personal projects. The production, usage, and disposal of these materials contribute to the overall burden of plastic waste.[11] 3D printing generates plastic waste in several channels. Failed prints, support structures, and prototypes contribute substantially to this waste.[12−14] It is estimated that approximately 30% of plastic utilized in 3D printing results in waste.[14] These materials accumulate and exacerbate the already critical issue of plastic pollution.

Received: September 11, 2025
Revised: October 30, 2025
Accepted: October 31, 2025
Published: November 25, 2025

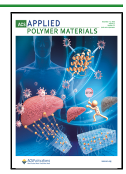

https://doi.org/10.1021/acsapm.5c02101
ACS Appl. Polym. Mater. 2025, 7, 16194−16205

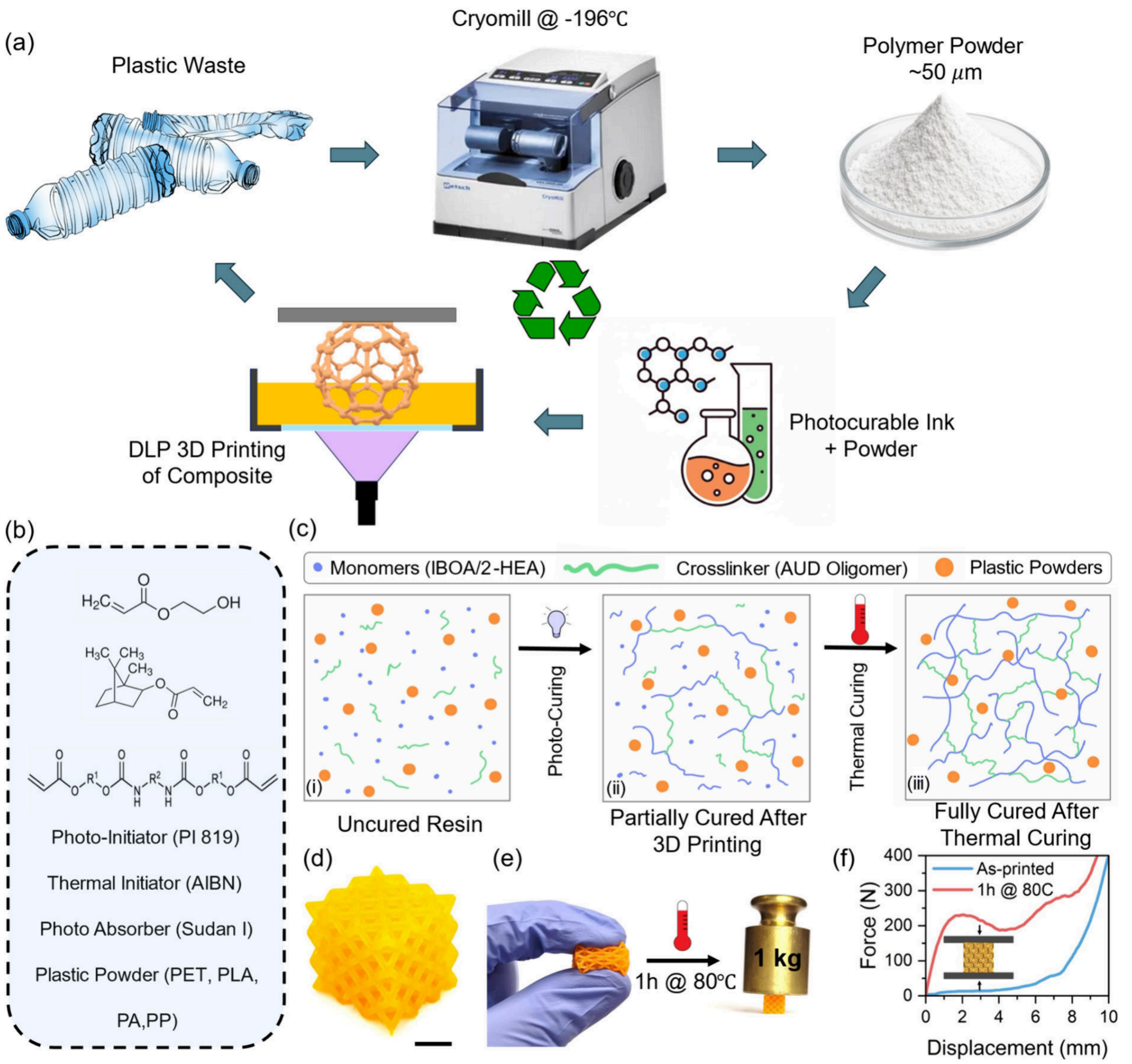

Figure 1. Illustration of composite preparation via DLP 3D printing using plastic waste powders. (a) Schematic workflow of milling plastic waste and incorporating the plastic powder into the DLP ink matrix for producing 3D objects. (b) Preparation of the used ink, which consists of 2-HEA, IBOA, and AUD molecules in addition of photoinitiator, photoabsorber, thermal initiator, and different plastic powders. (c) Schematic illustration of the chemical structure of the ink in different stages: (i) initial ink, (ii) after UV-curing, and (iii) after thermal curing. (d) Printed lattice with an I:P of 100:25. The scale bar is 5 mm. (e) The printed lattice squeezed with fingers since it is soft due to partial curing, and after thermal curing, the modulus increases significantly and can hold a significantly heavy load. (f) The compression test result of the printed lattice in as-printed and thermally cured states.

In recent years, research has focused on sustainability in AM. One of the primary approaches for improving sustainability in 3D printing is introducing renewable feedstocks.[14−16] Plant- and microorganism-derived biobased small molecules and polymers provide a viable source of precursors that can be modified and formulated into resins and inks for sustainable AM.[17] These alternative materials provide AM users with environmentally friendly manufacturing options. These materials include naturally occurring biopolymers (polysaccharides, proteins, and DNA) obtained from microbes, plants, and other organisms[18−22] and synthetic (bio)degradable polymers (polylactic acid (PLA), polyhydroxyalkanoates (PHAs), polycaprolactone (PCL), polybutylene succinate (PBS), etc.).[23−25] The third category is synthesis of small molecules from renewable sources as renewable resins for resin-based 3D printing techniques.[26−29] Among these, itaconic acid and its derivatives have recently emerged as versatile bio-based building blocks for vat photopolymerization resins. Their incorporation enables the design of photocurable systems with high bio-based content, competitive mechanical properties, and recyclability, highlighting their potential as sustainable alternatives to petrochemical acrylates.[30−34] However, in these approaches, plastics should be sorted first before they can be renewed, which is time-consuming and adds to the cost of the overall recycling process.[35,36]

Recycling and reprocessing are critical components of sustainable AM. These approaches are particularly well-studied in filament-based 3D printing techniques such as fused filament fabrication (FFF).[13,37−41] Plastic waste is ground, melted, and extruded to produce recycled filaments, which can then be used in the 3D printing process. This method not only helps to reduce plastic waste but also promotes the efficient use of materials, contributing to the overall sustainability of manufacturing practices.[42] However, it is noted that filaments of different material types cannot be mixed together before they can be reprocessed to form new filaments.

https://doi.org/10.1021/acsapm.5c02101
ACS Appl. Polym. Mater. 2025, 7, 16194−16205

The sustainability in the resin 3D printing process is more complicated due to the cross-linking nature of these AM techniques. Most materials produced via vat photopolymerization and its underlying techniques, such as digital light processing (DLP) or stereolithography (SLA), rely on cross-linked thermosets, which are traditionally nonreprocessable due to permanent covalent bonds.[43−45] Covalent adaptive networks (CANs) address this issue by incorporating dynamic bonds that can break and reconnect, enabling self-healing, reprocessing, and recycling without degrading mechanical properties.[46−48] Yue et al. advanced this concept with δ-lactone-based polymers that depolymerize to their monomers at ∼120 °C, avoiding the chain degradation common in conventional vitrimers.[49,50] This approach offers a viable path for reprocessable thermosets in resin-based 3D printing. However, recycling using CANs faces the challenge of balancing service and reprocessing temperatures. Complementary efforts have explored chemical recycling routes for vat photopolymerization, exemplified by the one-pot depolymerization−repolymerization of PET into photocurable copolyesters.[51] Such molecular-level strategies enable precise tuning of the polymer structure and excellent compatibility with photopolymer matrices, but they typically involve multiple synthesis steps, catalysts, and higher energy input. In contrast, the mechanically driven approach pursued in this work offers a simpler and solvent-free pathway that preserves the original polymer backbone and minimizes the processing energy. Together, chemical and mechanical recycling represent synergistic directions toward sustainable photopolymer systems, one emphasizing molecular design flexibility and the other practical scalability.

As the demand for sustainable solutions in 3D printing continues to grow, the development of innovative strategies is critical to address the pressing environmental challenges posed by plastic waste. In this study, we propose an approach for repurposing common thermoplastics as feedstock in resin 3D printing. Using cryogenic milling, the plastics are ground into powders about 50 μm in size and incorporated into acrylate-based inks for DLP 3D printing to create polymeric composites. Integrating recycled plastic powders into resin formulations is a promising yet underexplored approach in resin-based 3D printing, with significant potential to reduce plastic waste and resin consumption. A key advantage is its ability to incorporate mixed plastic powders without prior sorting, a major challenge in conventional recycling.[35,36] This streamlines processing and enables the use of heterogeneous waste streams, enhancing the scalability and practicality. Additionally, previously 3D-printed components with these powders can be recycled, supporting circular material use. Unlike traditional recycling, which is often limited to specific polymers, this method accommodates thermoplastics and thermosets, highlighting its potential for sustainable AM. However, the incorporation of these particles also introduces challenges, i.e., high powder concentrations increase ink viscosity, impairing printability, while low concentrations lead to sedimentation and uneven distribution. To address these challenges and maximize powder loading, we adjusted the resin composition to balance viscosity according to powder concentration. Additionally, we use a heated vat system to further reduce viscosity by warming the ink during DLP 3D printing, which allows for successful high powder loading (ink:powder (I:P) weight ratio of 100:62.5). Solid particles also impact UV-curing, as they can block light and cause incomplete polymerization. To resolve this, we implement a two-stage curing process: adding a thermal initiator to the ink and annealing samples postprinting at 80 °C. This annealing step completes polymerization in shaded regions, enhancing the mechanical properties of the 3D-printed composites. These innovations demonstrate the feasibility of using commodity plastics in resin-based AM, offering a pathway for sustainable AM practices.

RESULTS AND DISCUSSION

Workflow and Material Design. Figure 1a outlines the sustainable material preparation and DLP 3D printing workflow. The process begins with common commodity plastic waste materials, such as polyethylene terephthalate (PET), polypropylene (PP), polylactic acid (PLA), and polyamide (PA), which are processed into fine powders using cryogenic milling. These powders are then mixed with a photocurable ink made from acrylate-based monomers, acting as a filler. The resulting ink is used as the precursor for DLP 3D printing. Any unwanted 3D-printed objects or waste materials produced during the process can be ground back into powders and reused, achieving a circular manufacturing system.

Figure 1b shows the composition of the main ink (Ink1) in this study, which contains 45 wt % isobornyl acrylate (IBOA) and 35 wt % 2-hydroxyethyl acrylate (2-HEA) monomers and 20 wt % aliphatic urethane diacrylate oligomer (AUD) as cross-linker. AUD has high viscosity and serves as a viscosity modifier by increasing the viscosity of the ink, which can reduce the risk of sedimentation of powder in the resin, especially at low powder concentrations. This ink also includes 1 wt % photoinitiator (PI 819), 1 wt % azobis(isobutyronitrile) (AIBN) as a thermal initiator, and 0.05 wt % Sudan I as a photoabsorber. The plastic powder particles are included in the system with different ratios, and the resulting ink serves as the feedstock for the DLP 3D printing process, enabling the fabrication of powder-loaded composites. Postprinting, waste materials, including failed specimens and tested samples, can be cryogenically ground into fine powders for reuse. The chemical structures of the printed samples in different stages are schematically illustrated in Figure 1c. The presence of solid particles in the ink with relatively high concentration (>∼10 wt %) causes blocking of the UV light during the DLP process, which changes the curing state of the ink, leading to weaker properties of the 3D-printed objects. As schematically shown in Figure 1c(ii), the UV-curing during 3D printing is not effective in fully curing the resin, and some uncured monomers remain in the structure. The effect of solid particles on the curing percentage and curing depth is evaluated. The curing depth graph and scanning electron microscopy (SEM) images of the different samples are illustrated in Figure S1a−e. It is observed that as the powder weight ratio increases, the film thickness decreases due to the blocking of UV light. To further elucidate the light−ink interaction and rationalize the selected exposure parameters, the curing depth as a function of incident light dose was examined for both the neat resin and the powder-loaded formulation (Figure S1f). The neat resin exhibited the expected logarithmic increase in curing depth with increasing light dose, consistent with the Jacobs working-curve behavior.[52] In contrast, the powder-loaded samples showed a nearly constant curing depth regardless of energy input, confirming a pronounced light-blocking effect arising from scattering and absorption by the dispersed thermoplastic

https://doi.org/10.1021/acsapm.5c02101
ACS Appl. Polym. Mater. 2025, 7, 16194−16205

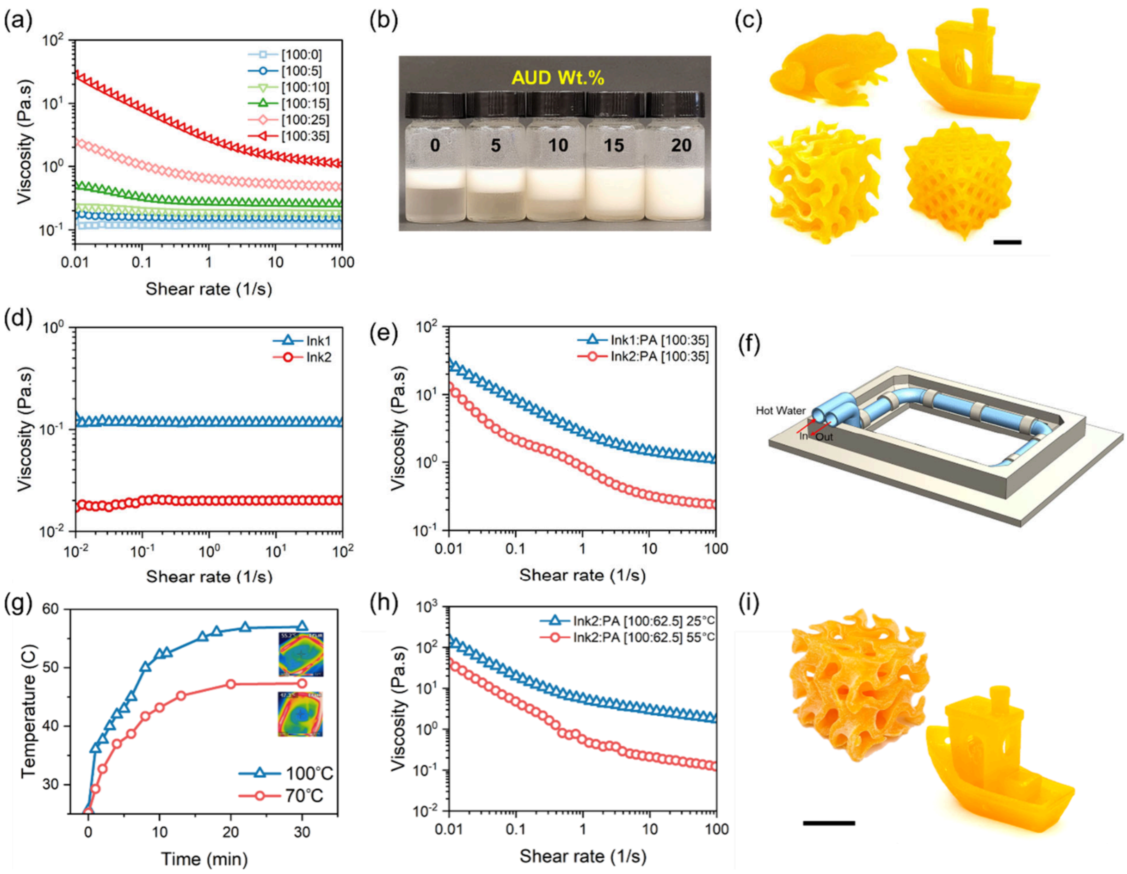

Figure 2. Viscosity measurement and printability of the powder-containing ink. (a) Viscosity of Ink1 with different powder contents (I:P from 100:0 to 100:35). (b) The stability evaluation of the ink/powder system in the presence of different ratios of AUD in the system after 6 months (the I:P is 100:10). (c) Printed objects from Ink1:PA with a ratio of 100:35 (scale bar is 5 mm). Comparison of viscosity between Ink1 and Ink2 in (d) the neat state and (e) with an I:P of 100:35. (f) Schematic representation of modified vat designed for heating the ink. (g) The temperature of the ink vs time in the heated vat with different water reservoir temperatures. (h) The viscosity of the systems with an I:P of 100:62.5 at different temperatures. (i) The printed objects from systems with an I:P of 100:62.5 at different at a vat temperature of 55 °C (scale bar is 10 mm).

particles. This attenuation behavior directly explains the reduced curing depth observed at higher powder loadings. Consequently, portions of the resin shielded by particles remain only partially polymerized, resulting in a lower stiffness compared to that of the neat resin printed under identical conditions. To address this issue, a thermal initiator is added to the ink, as illustrated schematically in Figure 1c(iii). Then, by annealing the printed objects for 1 h at 80 °C (at this temperature, the AIBN half-life is ∼1.2 h, ensuring efficient radical generation and polymerization), the mechanical properties are fully recovered. The printed object is even stiffer than the neat sample because these fillers are stiffer than the material from the neat resin. As shown in Figure 1d,e, the lattice printed with an I:P of 100:25 is very soft and can be easily squeezed by hand, while after being in 80 °C oven for 1 h, it can hold up to 1 kg of weight. Figure 1f shows the force−displacement curve in the compression test of the lattice at different conditions of as-printed and annealed at 80 °C for 1 h. It can be seen that the lattice immediately after printing is very soft, while thermal curing increases the stiffness of the sample dramatically. It is worth noting that post-thermal treatment was performed on fully printed specimens in a standard laboratory oven under ambient atmosphere. Because the reaction occurs predominantly in the bulk of the printed material, oxygen exposure is limited to the surface and has minimal influence on polymerization, as full conversion of the acrylate group after thermal treatment is confirmed by FTIR analysis. For clarity, the equivalent weight percentages of powder corresponding to the ink-to-powder ratios used in this study are given in Table S1.

Effects of Viscosity. The viscosity of the ink is a determinative characteristic that affects the print quality and properties of the final objects. Therefore, the viscosity of the ink with different ratios of powders is measured under different shear rates, as shown in Figure 2a. The neat ink shows Newtonian flow behavior, i.e., the viscosity is independent of shear rate. However, by introducing powder to the system, not only does the viscosity increase, but the flow behavior shifts to non-Newtonian as well, showing shear-thinning behavior, which is a common phenomenon in inks containing solid particles.

One of the primary challenges in formulating particle-laden ink lies in balancing the powder concentration and viscosity. If the viscosity of the ink is too low, powder sedimentation becomes a significant concern, particularly at low powder concentrations, which can lead to nonuniformity and defects in the final object. On the other hand, at high powder concentrations, the viscosity becomes too high, impairing the flow and printability of the ink. Thus, optimizing the ink formulation is crucial to achieving both suspension stability and suitable flow properties for effective processing. It is noted that Ink1 contains 20 wt % AUD, which is an oligomer that

https://doi.org/10.1021/acsapm.5c02101
ACS Appl. Polym. Mater. 2025, 7, 16194−16205

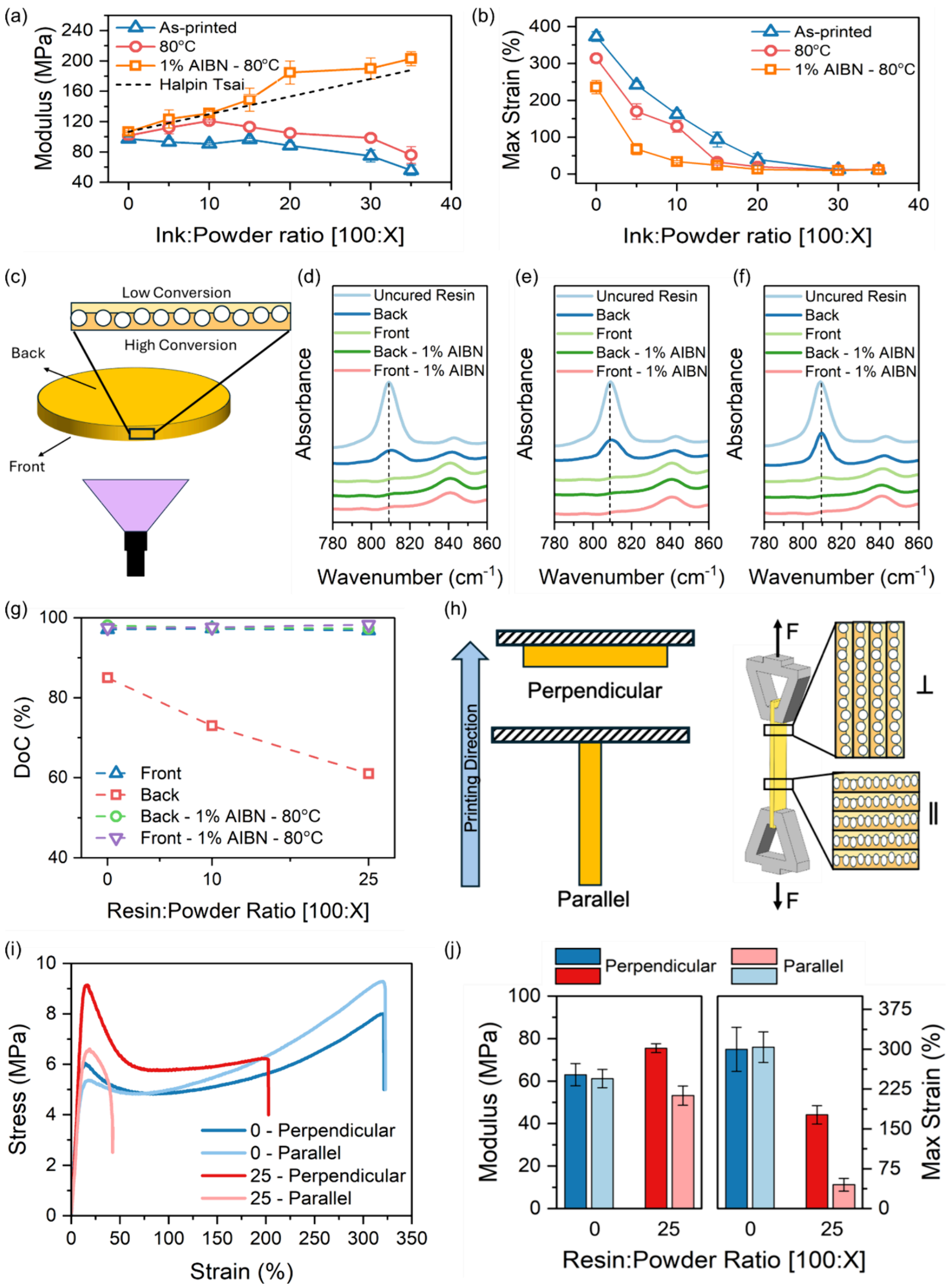

Figure 3. Mechanical properties and evaluation of the effect of solid particles on blocking the UV light during 3D printing process. (a) Young's modulus and (b) elongation at break of Ink1 with different concentrations of powder in three different states of as-printed, annealed at 80 °C for 1 h, and annealed at 80 °C for 1 h in the presence of 1 wt % AIBN thermal initiator. (c) Schematic representation of a cured disk designed to examine the blocking and scattering of UV light by powders in the matrix. The FTIR spectra of samples with an I:P of (d) 100:0, (e) 100:10, and (f) 100:25 in the range of 780−860 cm^{-1} in the uncured condition and from the back and front of the cured disk in two states of as-prepared and after annealing for 1 h at 80 °C. (g) DoC of the samples in different states obtained from FTIR spectra, specifically from monitoring the peak intensity of the C═C bond at ~809 cm^{-1}. (h) Schematic representation of the printed samples in different printing directions, perpendicular and parallel to the extension force in the tensile test experiment, along with a schematic diagram of the microstructure of the samples printed in different directions. (i) Stress−strain diagram and (h) Young's modulus and elongation at break of the neat sample and sample with an I:P of 100:25 printed in different directions.

elevates the ink viscosity remarkably. The content of AUD is rationally chosen to facilitate the powder stability and dispersion in the matrix. Increasing the viscosity of the ink helps stabilize the powder, which due to density mismatch tends to separate from the liquid phase. The colloidal stability of the resin suspensions was monitored over several months, during which no significant sedimentation or phase separation was observed. Minor settling that may occur over longer storage periods can be readily mitigated by brief shaking prior to use, consistent with a common practice for commercial resins. Figure 2b shows the inks with an I:P ratio of 100:10 and different AUD contents after sitting for six months. It can be seen that no visible phase separation is observed for the ink with 20 wt % AUD while it maintains good flowability, which is crucial for printability. Figure 2c shows different objects printed with the 100:35 ink, showing good print quality.

A further increase in the powder ratio, however, causes a significant increase in the viscosity. As a result, the ink cannot be used due to the lack of flowability. To address this issue, a new ink (Ink2) is formulated that only contains 7.5 wt % AUD (IBOA:2-HEA:AUD weight ratio = 30:62.5:7.5). This ink shows a relatively lower viscosity compared to Ink1 (Figure 2d). Figure 2e shows the viscosity of Ink1 and Ink2 in the presence of PA (I:P of 100:35). It can be observed that the viscosity of this system is reduced, and we are able to increase the I:P to 100:50.

To further increase the powder ratio in Ink2, the vat design is modified by incorporating a heating system. It consists of tubes surrounding the vat, as illustrated in Figure 2f, through which hot water flows, effectively raising the ink temperature and consequently reducing its viscosity. Detailed specifications of this heated vat system are provided in Figure S2. The ink temperature in this setup can be regulated by controlling the water temperature in the reservoir tank. Figure 2g displays the temperature profile of the heated vat at various time intervals, as measured by an infrared camera. This setup demonstrates the capability to heat the ink rapidly, achieving the desired temperature in less than 15 min. The maximum attainable ink temperature is dependent on the water temperature in the reservoir tank. The ink can be heated to 57 °C using boiling water in the reservoir, while a reservoir temperature of 70 °C results in a maximum ink temperature of 47 °C. It is worth mentioning that the ink temperature can be increased even more by using oil in the reservoir tank instead of water; however, very high temperatures are not favorable since these inks contain a thermal initiator (AIBN), which can be activated at temperatures above 65 °C.[53] By combining these modifications—utilizing lower viscosity ink and elevated temperatures—we successfully prepared inks with I:P ratios of up to 100:62.5 (or a powder concentration of 38.5 wt % of total ink). This improvement enabled the printing of complex objects with high powder loading, as demonstrated in Figure 2i.

Mechanical Properties. The mechanical properties of the printed composites are evaluated by printing dog-bone-shaped tensile specimens and applying an extension force with a strain rate of 0.015 s^{-1} parallel to the printing direction. For printing samples for mechanical property characterization, Ink1 with different PA powder concentrations is used. Figure 3a,b shows the Young's modulus and elongation at break for three types of samples, i.e., as-printed, printed without AIBN and annealed for 1 h at 80 °C, and printed with 1 wt % AIBN and then annealed at 80 °C for 1 h. Since the addition of the solid particles to the system creates composites, one would expect that the modulus of the samples should be higher than that of the neat samples. However, the samples in their as-printed condition show the opposite behavior. The addition of powder to the system up to an I:P of 100:15 does not change the modulus significantly, while above this ratio, the modulus drops remarkably. The modulus of the 100:35 sample in this condition drops ~42% compared to that of the neat sample (56 vs 97 MPa). The reason behind this phenomenon is the blocking of UV light by solid particles, which prevents the full conversion of some parts of the ink that are located behind the particles. In order to address this issue, we used a two-stage curing technique by adding 1 wt % AIBN to the ink and annealing the printed samples to complete the curing process. To have a reference for the thermal curing effect, the samples without thermal initiator are also annealed in the same thermal treatment. It can be observed that annealing the samples without AIBN slightly increases the modulus compared to the as-printed samples. The effect of annealing on the curing of the samples in the absence of the thermal initiator is investigated via FTIR experiments, and the results are shown in Figure S3. The FTIR spectrum of the partially cured sample of Ink1 in the as-printed condition is compared with the spectrum of the same sample annealed at 80 °C for 1 h. In our previous work, the thermal polymerization in acrylate-based monomers in the absence of a thermal initiator starts at significantly higher temperatures (above 150 °C).[4] The slight increase in the modulus in the composite samples might be due to improvement in the interface adhesion between the particles and matrix due to the elimination of gaps and voids between the particles and matrix via the diffusion of polymer chains around particles.[54,55]

On the other hand, the modulus of the samples with AIBN after thermal treatment increases significantly, approaching the theoretical values (dashed line in Figure 3a) calculated using the Halpin−Tsai model.[56,57] The 100:35 sample shows a modulus of 203 MPa (~265% recovery vs the unannealed sample). This demonstrates that the negative effect of solid particles on the mechanical properties in the system can be overcome by simple annealing of the samples with thermal initiators. It is important to note that the Halpin−Tsai model is based on idealized assumptions, including perfect particle−matrix adhesion, uniform particle dispersion, and well-defined particle geometry. Our system does not fully satisfy all of these conditions, however; interfacial debonding is observed for some thermoplastics (Figure S5), and the particle size distribution is polydisperse. Accordingly, the model is applied here as a first-order framework to qualitatively validate the observed modulus trends rather than as a rigorous quantitative predictor. While the Halpin−Tsai model provides a useful first-order estimation of composite stiffness, it presumes uniform particle geometry, perfect interfacial bonding, and homogeneous dispersion. In practice, the recycled polymer powders used in this study exhibit some degree of polydispersity in both size and shape, and SEM analysis reveals imperfect adhesion at the matrix−particle interface. These nonidealities reduce the efficiency of stress transfer between phases, resulting in experimentally measured moduli lower than the idealized predictions. Such discrepancies underscore the role of interfacial engineering and potential surface modification in achieving a mechanical performance closer to theoretical limits. Figure 3b shows the elongation vs powder content in the composite samples. It can be observed that in all samples, the presence of powder in the system reduces the elongation at break, which is due to the fact that the solid particles act as stress concentration areas in the system and that cracks can form from these areas and samples break in significantly smaller strains. On the other hand, the addition of AIBN in all samples (neat samples as well as composites) causes a drop in the elongation at break, which is due to the formation of a cross-linking structure in the samples, reducing their flexibility.

To further evaluate the influence of solid particles in the matrix, we designed an experiment to monitor the monomer conversion in different areas of the samples. For this purpose, 2 mL of liquid resin is applied to a glass slide and cured for 30 s by exposure to UV light from below, as shown in Figure 3c. We hypothesize that the presence of solid particles in the ink

https://doi.org/10.1021/acsapm.5c02101
ACS Appl. Polym. Mater. 2025, 7, 16194−16205

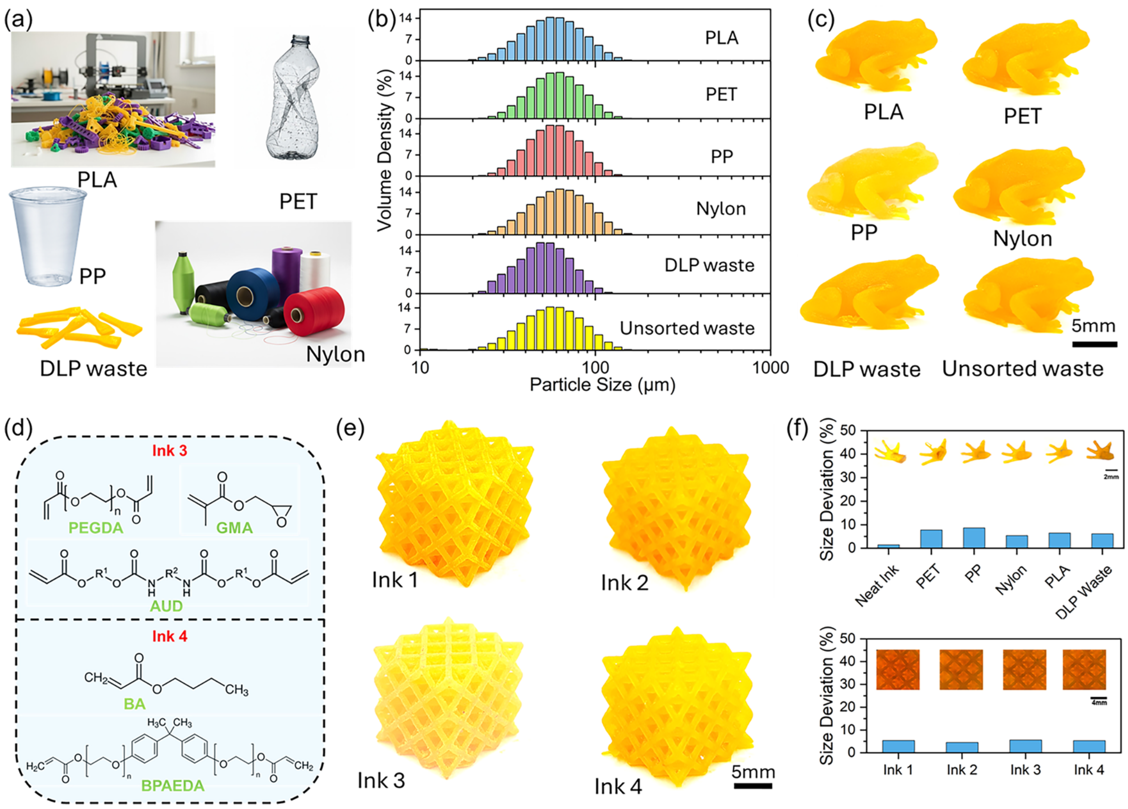

Figure 4. Expandability of this manufacturing process to different ink/powder systems. (a) The original waste materials used for fabrication of different polymeric powders in cryogenic milling, including PLA, PET, PP, nylon, and DLP 3D printing waste material. (b) The particle size distribution of the prepared powders from different plastic wastes. (c) Printed objects from Ink1 and different powders with an I:P of 100:25 to demonstrate the printability of different systems. (d) The composition of two additional inks (Ink3 and Ink4) to demonstrate versatility of this process with various ink/powder systems. (e) Printed objects from four different inks in this study including nylon powder with an I:P of 100:25. (f) The size deviation of the printed objects with different ink/powder systems compared to the dimensions of the original models used to print these objects.

blocks UV light, leading to lower monomer conversion behind the particles (back of the sample). Pure inks as well as inks with I:P ratios of 100:10 and 100:25 are used. The FTIR spectra of these samples in their uncured state, as well as from the front and back of the cured films, are shown in Figure 3d–f. Monomer conversion is assessed by monitoring the peak at ~809 cm^{-1}, corresponding to the C═C bond, whose intensity is used to quantify monomer conversion. The carbonyl peak at ~1720 cm^{-1} is used as a reference for calculating the degree of conversion (DoC). The monomer conversions at different surfaces are plotted in Figure 3g. In all three samples, the peak at ~809 cm^{-1} nearly disappears on the front face, which is most exposed to UV light, showing approximately 97% DoC. However, on the back face, the intensity of this peak does not drop to zero. The neat sample exhibits the smallest peak, corresponding to 85% conversion, while the 100:25 sample shows the largest peak, indicating only 61% DoC. The lower conversion in the neat ink is attributed to the presence of Sudan I, which absorbs UV light, preventing full curing of the monomer at the back in these relatively thick samples (~0.5 mm). In contrast, samples with powder exhibit a significantly higher difference between the front and back with the polymer at the back being only partially cured. This is due to the blocking effects of the solid particles in the matrix. To address this, another set of samples is prepared with 1 wt % AIBN, followed by 1 h annealing at 80 °C. The FTIR spectra of these thermally annealed samples show that the acrylate C═C bond has almost entirely disappeared (Figure 3d–f), and the DoC for both the front and back of the samples is ~97% for all three compositions (Figure 3g). This confirms that thermal annealing effectively eliminates partial conversion in the system and ensures a fully cured structure. It is worth mentioning that since 80 °C is far below the melting temperatures of PLA, PA, PP, and PET, the particulate phase is not expected to undergo melting or phase transitions. Near-complete consumption of residual acrylate double bonds (confirmed by FTIR) indicates that property gains arise from increased matrix conversion rather than particle changes.

Another experiment is designed to further evaluate this phenomenon and its influence on the mechanical properties of the printed samples. We used neat ink as a reference and 100:25 ink for the printing composites. Two sets of rectangular tensile bars are printed in two different directions, horizontal and vertical, as shown in Figure 3h. For samples printed in the vertical direction, the applied force during the tensile test is parallel to the printing direction, while for samples printed in the horizontal direction, the applied force is perpendicular to the printing direction. From Figure 3i it can be seen that in the neat sample, the influence of the printing direction on the mechanical properties is negligible, while in the 100:25 composite, the mechanical properties significantly depend on the printing direction. Printing samples perpendicular to the extension direction causes a 42% increase in Young's modulus and a 292% increase in elongation at break compared to

https://doi.org/10.1021/acsapm.5c02101
ACS Appl. Polym. Mater. 2025, 7, 16194−16205

samples printed parallel to the force direction (Figure 3j). This dramatic difference in the mechanical properties can be explained by using the schematic in Figure 3h. Due to the layer-by-layer nature of DLP 3D printing, in these composite samples, there is a layered structure of fully cured and partially cured material due to the blocking effect of solid particles in the structure, and the partially cured material shows weaker mechanical properties. In the parallel configuration, the partially cured layers expand across the cross section of the sample; as the load is more likely to cause delamination or failure at the interfaces between the fully and partially cured layers, it therefore leads to a lower strength and modulus of the sample in the tensile test.[58,59] This behavior resembles the Reuss model in composite mixture theory, where the softer phase dominates the deformation response, reducing overall stiffness.[60] On the other hand, in the sample printed perpendicular to the printing direction, the layers expand in the direction of force, and there are continuous phases of cured sample that expand from one end to the other; the load is thus distributed along these fully cured segments of the sample, which compensate for the weaker layers between them.[61] This behavior is more consistent with the Voigt model, where the stiffer phase carries most of the load, resulting in higher modulus and strength.[60] It should be noted that Figure 3i,j is shown before thermal curing and thus captures the presence of partially cured regions arising from light attenuation, which underlies the observed anisotropy.

Different Ink/Powder Systems. To validate our process for various ink and powder systems, we utilized cryogenic milling to produce powders from PLA, sourced from the waste material of FFF 3D printers; PET, derived from water and soda bottles; PP, from plastic cups; nylon powder, provided by HP, Inc.; and DLP 3D printing waste material (Figure 4a). In addition to individually ground powders, one powder sample is achieved by grinding all plastics (including PLA, PET, PP, nylon, and DLP-printed sample) together as an unsorted sample. These powders were subsequently mixed with inks formulated from different monomer combinations. The particle size distributions of these powders are presented in Figure 4b. The average particle size for thermoplastic sourced powders ranges from 58.1 to 62.5 μm, while the DLP waste sourced powder shows a powder range of 45−50 μm. All powders showed a nearly normal distribution. Figure S4 illustrates the viscosity of samples prepared with Ink1, containing an I:P ratio of 100:25 with different powders. The flow behavior of these systems is similar, likely due to the comparable particle size distributions. Figure 4c demonstrates the printability of Ink1 with different powders for printing complex and relatively small samples. In these set experiments, the I:P is 100:25. The distribution of these powders in the matrix of the composite is examined via SEM analysis. The fracture surface of the samples is analyzed, and the results are presented in Figure S5a−f. The SEM images suggest a uniform distribution of the powders across all samples. Compared with other thermoplastic powders, the DLP waste particles produced composites with smoother fracture surfaces. Although the average particle size was ∼10% smaller, we attribute the main effect to favorable surface chemistry and higher compatibility with the acrylate matrix, which improved wetting and interfacial adhesion during curing. The smoother fracture surfaces observed for the DLP waste composites indicate improved interfacial adhesion. To validate the impact of this particle−matrix compatibility, we compared the tensile behavior of composites with PA and DLP waste with an I:P of 100:25 (Figure S6). The results confirm that while rigid particle addition reduces stretchability overall, the DLP waste composite maintains substantially higher elongation compared to PA, supporting improved compatibility with the resin matrix. Surface chemistry modification of the polymer particles could further enhance particle−matrix adhesion and thereby improve mechanical properties. Such interfacial optimization is particularly important for mitigating the stiffness−ductility trade-off observed in particle-filled systems. Enhanced bonding can promote more uniform stress transfer and delay crack initiation, improving toughness without compromising stiffness. In practical terms, controlling interfacial chemistry allows tailoring of the composite response for distinct applications, favoring higher rigidity in structural parts or greater elasticity in functional and energy-absorbing components.

One of the notable advantages of this approach is its ability to incorporate mixed plastic powders without requiring prior sorting, which is a major challenge in traditional recycling processes due to the high cost and complexity of separation. This feature improves both the efficiency and the scalability of the method, allowing for the direct utilization of heterogeneous plastic waste streams. Additionally, it enables the reuse of previously printed components containing these powders, further extending the material life-cycle. Unlike conventional recycling techniques, which are often constrained to thermoplastics, such as mechanical recycling that depends on remelting and reprocessing, this method offers greater flexibility by accommodating a variety of polymer types, including thermoplastics, thermosets, and cross-linked materials. These attributes reinforce the practicality of incorporating recycled plastic powders into resin-based systems, making this a promising avenue for advancing sustainable additive manufacturing.

To further evaluate the versatility of this method, along with the two primary inks used in this study, two additional ink formulations are developed, as shown in Figure 4d: Ink3 contains poly(ethylene glycol) diacrylate (PEGDA), glycidyl methacrylate (GMA), and AUD with a weight ratio of PEGDA:GMA:AUD = 40:40:20, and Ink4 contains butyl acrylate (BA) and bisphenol A ethoxylate diacrylate (BPAEDA) with a weight ratio of BA:BPAEDA = 80:20. The content of other reagents (photoinitiator and photoabsorber) in these inks is similar to that in Ink1. Figure S7 presents the viscosities of the various inks as a function of the shear rate, indicating a wide range of viscosities across the different formulations. Figure 4e shows the printability of different inks (Ink1, Ink2, Ink3, and Ink4) in the presence of PA powder with a ratio of 100:25. From these images, it could be observed that this technique can be expanded to many different ink/powder systems easily. The acrylate-based resins used in this work serve as a representative system to demonstrate the feasibility of incorporating thermoplastic powders into DLP-printable resins. The formulation is not tailored for a specific application but chosen to enable particle incorporation and curing. The general approach is transferable to resins of different chemical compositions. In order to evaluate the accuracy of the printing process, we measure the size of different areas and features of the printed samples, compare them with the original slices used to print these objects, and calculate the size deviation. It can be observed that in all systems, deviation from the model is not significant (4−7%). The results in this section suggest that this strategy is versatile and can be expanded to different polymeric particles as well as different photopolymerizable inks and that it can create complex structures with the DLP 3D printing technique with high accuracy.

A potential challenge associated with this technique is the weak adhesion of surface particles to the printed samples. A small fraction of particles remain loosely attached, which may detach after printing and lead to issues such as contamination, surface defects, or inconsistencies in subsequent processing steps. To mitigate this, a postprocessing treatment was implemented, wherein the printed samples were exposed to UV light under an inert nitrogen atmosphere. This exposure facilitates surface curing, enhancing the adhesion of these particles and reducing the risk of detachment, thereby improving the overall reliability and consistency of the printed structures. Moreover, in formulating particle-filled resins for vat photopolymerization, several physicochemical parameters should be considered. Resin viscosity affects both suspension stability and printability. Particle−matrix compatibility influences interfacial adhesion and composite performance. Curing kinetics can be impacted by particle-induced light scattering, and storage stability must be ensured for practical use. These factors are broadly applicable across different resin chemistries and help to highlight the versatility of the approach demonstrated here.

Beyond formulation aspects, the environmental and energetic implications of the proposed process were also considered to assess its potential sustainability benefits. The Retsch CryoMill instrument employed for polymer powder preparation operates with a nominal electrical power of 260 W and low liquid-nitrogen (LN_2) consumption according to manufacturer data. Industrial cryogenic milling systems have been reported to require approximately 0.5 kg of LN_2 per kg of processed polymer,[62] corresponding to an overall energy input of 0.7−2.0 MJ kg^{-1} when accounting for the 0.36−0.55 kWh kg^{-1} electricity needed for LN_2 production.[63] In this work, up to 40 wt % of the resin formulation was composed of recycled thermoplastic powder, effectively halving the demand for virgin acrylate monomers, whose production typically requires 60−80 MJ kg^{-1} of embodied energy.[64] This substitution therefore offers an estimated 30−35 MJ kg^{-1} reduction in material energy demand. When considered alongside previously reported life-cycle analyses for photopolymer systems,[65] these estimations highlight that the demonstrated process provides a quantitatively favorable sustainability profile with further potential gains upon scale-up.

Despite the promising performance achieved, several challenges remain before sustainable DLP can be broadly implemented. Improving interfacial compatibility between the dispersed recycled thermoplastic phase and the photocurable matrix is essential to further enhance toughness and elongation without compromising stiffness. Moreover, large-scale adoption will depend on the economic viability of recycling and formulation processes, which calls for cost−benefit and life-cycle assessments to guide process optimization. Looking ahead, opportunities lie in integrating hybrid recycling approaches that combine mechanical and chemical valorization routes, the development of reactive surface treatments to improve phase adhesion, and the use of bio-derived or low-energy photoinitiator systems. The convergence of sustainable chemistry, digital process control, and data-driven resin design may ultimately enable scalable circular DLP manufacturing.

CONCLUSION

In this study, we propose a strategy for sustainable AM by utilizing common plastic wastes in the form of fine powders as feedstock for resin-based 3D printing to fabricate polymeric composites. PET, PLA, PP, and PA separately and in mixed conditions are cryogenically ground to powders with an average particle size of 50−60 μm. These resultant powders are then mixed with a DLP ink, which comprises a blend of various monomers and cross-linkers, and used as the resin to print various objects. After printing, the resulting composites are cryogenically ground again and reintroduced as feedstocks in the DLP resin, establishing a circular recycling workflow. The incorporation of solid particles into the ink significantly elevates its viscosity, limiting the maximum powder loading to a weight ratio of 100:35 (I:P). To address this challenge, we employ two strategies: first, we reduce the viscosity of the ink, which is initially increased to enhance powder stability at lower concentrations; second, we use a heated vat system to raise the temperature of the ink to 55 °C during printing, consequently reducing the ink viscosity. These adjustments enabled us to increase the powder loading to a weight ratio of 100:62.5. The presence of solid particles in the resin during printing affects the process by blocking UV light, leading to lower conversion rates in areas shielded by the particles. To mitigate this issue, we propose a two-stage curing process by incorporating 1 wt % of a thermal initiator into the ink and annealing the samples postprinting at 80 °C for 1 h. This thermal curing approach proves to be a promising solution, leading to a 265% increase in the modulus of samples with a 100:35 I:P compared to their as-printed condition, which initially exhibits a modulus nearly 50% lower than that of the neat sample. This work establishes a circular recycling framework for resin-based 3D printing, offering a practical approach to reducing plastic waste in manufacturing. Furthermore, the methodologies introduced in this study, such as the heated vat system and two-stage curing process to enhance mechanical properties, demonstrate broad applicability and can be used for other ink and powder systems, paving the way for the fabrication of diverse composite materials in advanced resin-based additive manufacturing techniques.

EXPERIMENTAL SECTION

DLP Inks. In this study, different photocurable inks have been used for the preparation of the composites that are achieved by mixing different acrylate-based monomers and cross-linkers. Ink1 includes isobornyl acrylate (IBOA), 2-hydroxyethyl acrylate (2-HEA), and aliphatic urethane diacrylate oligomer (AUD) with a weight ratio of IBOA:2-HEA:AUD = 45:35:20. Ink2 contains IBOA, 2-HEA, and AUD with a weight ratio of IBOA:2-HEA:AUD = 30:62.5:7.5. Ink3 is a mixture of polyethylene glycol diacrylate, Mn = 250 (PEGDA), glycidyl methacrylate (GMA), and AUD with a weight ratio of PEGDA:GMA:AUD = 40:40:20. Ink4 includes butyl acrylate (BA) and bisphenol A ethoxylate diacrylate, Mn = 512 (BPAEDA), with a weight ratio of BA:BPAEDA = 80:20. All inks include 1 wt % photoinitiator (Irgacure 819) and 0.05 wt % photoabsorber (Sudan I). All of the above chemicals except for Ebecryl 8413, which is provided by Allnex (Alpharetta, GA, USA), are purchased from Sigma-Aldrich (St. Louis, MO, USA) and used as received. Isopropyl alcohol (IPA) for cleaning of the 3D-printed samples is purchased from VWR (Radnor, PA, USA).

Powder Preparation. The PLA, PET, and PP powders used in this study are achieved via cryogenic milling of common plastic materials such as water bottles, disposable plastic cups, and FFF 3D printer waste materials. A cryomill (Retsch GmbH, Haan, Germany) equipped with a 50 mL jar is used to grind the powders under liquid nitrogen. Samples are first precooled for 2 min under cryogenic conditions, followed by grinding with a ball-to-powder ratio of approximately 9:1 by weight. Milling is carried out in two cycles of 5 min each. These parameters are selected to ensure reproducibility and consistent particle size reduction. Nylon powder is provided by HP, Inc. (Palo Alto, CA, USA). It is worth mentioning that thermoplastic powders (PP, PLA, PA, and PET) are selected based on preliminary compatibility tests, in which no significant dissolution or swelling is observed when dispersed in the acrylate-based resin. This ensured the formation of particulate-filled composites rather than blended systems. In contrast, other plastic powders, such as polyethylene (PE) and polystyrene (PS), exhibit partial dissolution or swelling and are excluded to preserve the intended composite morphology.

Powder Characterization. A laser diffraction particle size analyzer (Mastersizer 3000, Malvern Instruments Ltd., Worcestershire, UK) equipped with an Aero S dry powder dispersion attachment is used to determine the particle size distribution of the powders. The device's software, utilizing Mie theory, calculates the distribution from the light scattering pattern. The software also automatically computes the particle size distributions at 10% (Dv10), 50% (Dv50, or median diameter), and 90% (Dv90) of the volume distribution based on Fraunhofer theory. Each measurement is repeated five times.

3D Printing. 3D printing is performed with a bottom-up DLP printer that employs a 385 nm UV-LED light projector (PRO4500, Wintech Digital Systems Technology Corp., Carlsbad, CA, USA) and a linear translation stage (LTS150 Thorlabs, Newton, NJ, USA). A homemade container with an oxygen-permeable window (Teflon AF-2400, Vici Metronics Inc., Poulsbo, WA, USA) is used as the resin vat. Samples are printed by using a DLP 3D printer with a layer thickness of 50 μm and an exposure time of 3 s per layer. After printing, all samples are developed with isopropyl alcohol followed by postcuring under UV light at an intensity of ~40 mW/cm^2 for 1 min per side to ensure complete surface curing. The light intensity of the printer is calibrated with a photometer (ILT1400-A Radiometer, International Light Technologies Inc., MA, USA) before printing. The heated vat is also designed and manufactured in our lab. The resin in the vat is heated by the circulation of hot water in a tube located at the inner edges of the vat connected to a DC pump and a boiling water reservoir.

Property Characterization. The uniaxial tension tests are performed with a universal test machine (Insight 10, MTS Systems Corp., Eden Prairie, MN, USA) with a cross-head speed of 5 mm/min. The degree of curing is decided by the normalized FTIR (Nicolet iS50 spectrometer, Thermo Fisher Scientific, Waltham, MA, USA) peak intensity of the acrylate group present at 809 cm^{-1}. Multiple tests are conducted for each sample to guarantee reproducibility. A scanning electron microscope (SU8230, Hitachi, Japan) is used to analyze the morphology of the samples. To assess the particle size distribution within the matrix, the cross section of samples fractured under liquid nitrogen is examined under SEM. For curing depth analysis, the thickness of cured thin films on a glass slide is measured using SEM imaging, ensuring accurate thickness determination. The curing depth of the samples with different powder concentrations is measured using scanning electron microscopy (SEM) imaging. For this purpose, 2 mL of ink containing various concentrations of PA is applied to a glass slide and cured by shining UV light (25 mW/cm^2) from the bottom for 20 s. After the curing process, the samples are peeled off, and their thicknesses are measured using SEM imaging.

Rheological Properties. Rheological measurements are performed on a DHR-3 rheometer (TA Instruments, New Castle, DE, USA) equipped with a double-walled concentric cylinder geometry. The measurements are taken at 25 and 50 °C using a shear rate sweep between 0.01 and 100 s^{-1}.

■ ASSOCIATED CONTENT

Supporting Information

The Supporting Information is available free of charge at https://pubs.acs.org/doi/10.1021/acsapm.5c02101.

Additional figures and data, including curing depth analysis of powder-loaded resins; schematic and images of the heated vat system; FTIR spectra evaluating annealing effects; viscosity measurements under various conditions; SEM images of fracture surfaces for different powders; mechanical property comparison of composites for powders with different surface chemistries; and a conversion table correlating ink-to-powder ratios with weight percentages (PDF)

■ AUTHOR INFORMATION

Corresponding Author

Hang Jerry Qi − *The George W. Woodruff School of Mechanical Engineering, Georgia Institute of Technology, Atlanta, Georgia 30332, United States; School of Materials Science and Engineering, Georgia Institute of Technology, Atlanta, Georgia 30332, United States;* orcid.org/0000-0002-3212-5284; Email: qih@me.gatech.edu

Authors

Farzad Gholami − *The George W. Woodruff School of Mechanical Engineering, Georgia Institute of Technology, Atlanta, Georgia 30332, United States; School of Materials Science and Engineering, Georgia Institute of Technology, Atlanta, Georgia 30332, United States*

Mingzhe Li − *The George W. Woodruff School of Mechanical Engineering, Georgia Institute of Technology, Atlanta, Georgia 30332, United States*

Alvaro Hucker − *The George W. Woodruff School of Mechanical Engineering, Georgia Institute of Technology, Atlanta, Georgia 30332, United States*

Summer Clark − *The George W. Woodruff School of Mechanical Engineering, Georgia Institute of Technology, Atlanta, Georgia 30332, United States; Coretta Scott King Young Women's Leadership Academy, Atlanta, Georgia 30318, United States*

Frédéric Demoly − *ICB UMR 6303 CNRS, Université Marie et Louis Pasteur, UTBM, 90010 Belfort Cedex, France; Institut universitaire de France (IUF), 75231 Paris, France*

Kun Zhou − *Singapore Centre for 3D Printing, School of Mechanical and Aerospace Engineering, Nanyang Technological University, Singapore 639798, Singapore;* orcid.org/0000-0001-7660-2911

Complete contact information is available at: https://pubs.acs.org/10.1021/acsapm.5c02101

Notes

The authors declare no competing financial interest.

■ REFERENCES

(1) Nature. On the plastics crisis. *Nature Sustainability* **2023**, *6* (10), 1137.

(2) MacLeod, M.; Arp, H. P. H.; Tekman, M. B.; Jahnke, A. The global threat from plastic pollution. *Science* **2021**, *373* (6550), 61−65.

(3) Li, M.; Gholami, F.; Yue, L.; Fratarcangeli, M. R.; Black, E.; Shimokawa, S.; Nomura, T.; Tanaka, M.; Kobayashi, H.; Song, Y.; et al. Coaxial-Spun Hollow Liquid Crystal Elastomer Fiber as a Versatile Platform for Functional Composites. *Adv. Funct. Mater.* **2024**, *34* (42), 2406847.

(4) Gholami, F.; Yue, L.; Li, M.; Jain, A.; Mahmood, A.; Fratarcangeli, M.; Ramprasad, R.; Qi, H. J. Fast and Efficient Fabrication of Functional Electronic Devices through Grayscale Digital Light Processing 3D Printing. *Adv. Mater.* **2024**, *36* (46), 2408774.
(5) Pang, Y.; Cao, Y.; Chu, Y.; Liu, M.; Snyder, K.; MacKenzie, D.; Cao, C. Additive Manufacturing of Batteries. *Adv. Funct. Mater.* **2020**, *30* (1), 1906244.
(6) Tofail, S. A. M.; Koumoulos, E. P.; Bandyopadhyay, A.; Bose, S.; O'Donoghue, L.; Charitidis, C. Additive manufacturing: scientific and technological challenges, market uptake and opportunities. *Mater. Today* **2018**, *21* (1), 22−37.
(7) Ngo, T. D.; Kashani, A.; Imbalzano, G.; Nguyen, K. T. Q.; Hui, D. Additive manufacturing (3D printing): A review of materials, methods, applications and challenges. *Composites Part B: Engineering* **2018**, *143*, 172−196.
(8) Vafadar, A.; Guzzomi, F.; Rassau, A.; Hayward, K. Advances in Metal Additive Manufacturing: A Review of Common Processes, Industrial Applications, and Current Challenges. *Applied Sciences* **2021**, *11*, 1213.
(9) Park, S.; Shou, W.; Makatura, L.; Matusik, W.; Fu, K. 3D printing of polymer composites: Materials, processes, and applications. *Matter* **2022**, *5* (1), 43−76.
(10) Islam, M. A.; Mobarak, M. H.; Rimon, M. I. H.; Al Mahmud, M. Z.; Ghosh, J.; Ahmed, M. M. S.; Hossain, N. Additive manufacturing in polymer research: Advances, synthesis, and applications. *Polym. Test.* **2024**, *132*, 108364.
(11) Rodríguez-Hernández, A. G.; Chiodoni, A.; Bocchini, S.; Vazquez-Duhalt, R. 3D printer waste, a new source of nanoplastic pollutants. *Environ. Pollut.* **2020**, *267*, 115609.
(12) Hegab, H.; Khanna, N.; Monib, N.; Salem, A. Design for sustainable additive manufacturing: A review. *Sustainable Materials and Technologies* **2023**, *35*, No. e00576.
(13) Balou, S.; Ahmed, I.; Priye, A. From Waste to Filament: Development of Biomass-Derived Activated Carbon-Reinforced PETG Composites for Sustainable 3D Printing. *ACS Sustainable Chem. Eng.* **2023**, *11* (34), 12667−12676.
(14) Zhu, C.; Li, T.; Mohideen, M. M.; Hu, P.; Gupta, R.; Ramakrishna, S.; Liu, Y. Realization of Circular Economy of 3D Printed Plastics: A Review. *Polymers* **2021**, *13*, 744.
(15) Sanchez-Rexach, E.; Johnston, T. G.; Jehanno, C.; Sardon, H.; Nelson, A. Sustainable Materials and Chemical Processes for Additive Manufacturing. *Chem. Mater.* **2020**, *32* (17), 7105−7119.
(16) Guggenbiller, G.; Brooks, S.; King, O.; Constant, E.; Merckle, D.; Weems, A. C. 3D Printing of Green and Renewable Polymeric Materials: Toward Greener Additive Manufacturing. *ACS Applied Polymer Materials* **2023**, *5* (5), 3201−3229.
(17) Zhu, Y.; Romain, C.; Williams, C. K. Sustainable polymers from renewable resources. *Nature* **2016**, *540* (7633), 354−362.
(18) Li, V. C.-F.; Dunn, C. K.; Zhang, Z.; Deng, Y.; Qi, H. J. Direct Ink Write (DIW) 3D Printed Cellulose Nanocrystal Aerogel Structures. *Sci. Rep.* **2017**, *7* (1), 8018.
(19) Li, V. C. F.; Mulyadi, A.; Dunn, C. K.; Deng, Y.; Qi, H. J. Direct Ink Write 3D Printed Cellulose Nanofiber Aerogel Structures with Highly Deformable, Shape Recoverable, and Functionalizable Properties. *ACS Sustainable Chem. Eng.* **2018**, *6* (2), 2011−2022.
(20) Maniglia, B. C.; Lima, D. C.; Matta Junior, M. D.; Le-Bail, P.; Le-Bail, A.; Augusto, P. E. D. Hydrogels based on ozonated cassava starch: Effect of ozone processing and gelatinization conditions on enhancing 3D-printing applications. *Int. J. Biol. Macromol.* **2019**, *138*, 1087−1097.
(21) Jia, J.; Richards, D. J.; Pollard, S.; Tan, Y.; Rodriguez, J.; Visconti, R. P.; Trusk, T. C.; Yost, M. J.; Yao, H.; Markwald, R. R.; et al. Engineering alginate as bioink for bioprinting. *Acta Biomaterialia* **2014**, *10* (10), 4323−4331.
(22) Davidenko, N.; Hamaia, S.; Bax, D. V.; Malcor, J.-D.; Schuster, C. F.; Gullberg, D.; Farndale, R. W.; Best, S. M.; Cameron, R. E. Selecting the correct cellular model for assessing of the biological response of collagen-based biomaterials. *Acta Biomaterialia* **2018**, *65*, 88−101.
(23) Nemati Hayati, A.; Hosseinalipour, S. M.; Rezaie, H. R.; Shokrgozar, M. A. Characterization of poly(3-hydroxybutyrate)/nano-hydroxyapatite composite scaffolds fabricated without the use of organic solvents for bone tissue engineering applications. *Materials Science and Engineering: C* **2012**, *32* (3), 416−422.
(24) Elomaa, L.; Teixeira, S.; Hakala, R.; Korhonen, H.; Grijpma, D. W.; Seppälä, J. V. Preparation of poly(ε-caprolactone)-based tissue engineering scaffolds by stereolithography. *Acta Biomaterialia* **2011**, *7* (11), 3850−3856.
(25) Bose, S.; Ke, D.; Sahasrabudhe, H.; Bandyopadhyay, A. Additive manufacturing of biomaterials. *Prog. Mater. Sci.* **2018**, *93*, 45−111.
(26) Weems, A. C.; Delle Chiaie, K. R.; Worch, J. C.; Stubbs, C. J.; Dove, A. P. Terpene- and terpenoid-based polymeric resins for stereolithography 3D printing. *Polym. Chem.* **2019**, *10* (44), 5959−5966.
(27) Guit, J.; Tavares, M. B. L.; Hul, J.; Ye, C.; Loos, K.; Jager, J.; Folkersma, R.; Voet, V. S. D. Photopolymer Resins with Biobased Methacrylates Based on Soybean Oil for Stereolithography. *ACS Applied Polymer Materials* **2020**, *2* (2), 949−957.
(28) Voet, V. S. D.; Strating, T.; Schnelting, G. H. M.; Dijkstra, P.; Tietema, M.; Xu, J.; Woortman, A. J. J.; Loos, K.; Jager, J.; Folkersma, R. Biobased Acrylate Photocurable Resin Formulation for Stereolithography 3D Printing. *ACS Omega* **2018**, *3* (2), 1403−1408.
(29) Ding, R.; Du, Y.; Goncalves, R. B.; Francis, L. F.; Reineke, T. M. Sustainable near UV-curable acrylates based on natural phenolics for stereolithography 3D printing. *Polym. Chem.* **2019**, *10* (9), 1067−1077.
(30) Maturi, M.; Spanu, C.; Maccaferri, E.; Locatelli, E.; Benelli, T.; Mazzocchetti, L.; Sambri, L.; Giorgini, L.; Franchini, M. C. (Meth)acrylate-Free Three-Dimensional Printing of Bio-Derived Photocurable Resins with Terpene- and Itaconic Acid-Derived Poly(ester-thioether)s. *ACS Sustainable Chem. Eng.* **2023**, *11* (49), 17285−17298.
(31) Schulz, N. M.; Papadopoulos, L.; Hagenlocher, L.; Gohla, A.; Bikiaris, D. N.; Robert, T. Wood and olive kernel flour as reinforcement for itaconic acid-based UV-curing additive manufacturing material. *React. Funct. Polym.* **2025**, *208*, 106161.
(32) Huang, W.; Zu, Z.; Huang, Y.; Xiang, H.; Liu, X. UV-curing 3D printing of high-performance, recyclable, biobased photosensitive resin enabled by dual-crosslinking networks. *Additive Manufacturing* **2024**, *91*, 104352.
(33) Maturi, M.; Maturi, S.; Sanz de León, A.; Migliorini, L.; de la Mata, M.; Benelli, T.; Giorgini, L.; Milani, P.; Comes Franchini, M.; Molina, S. I. Enhanced Properties of 3D-Printed Graphene Oxide Nanocomposites through Itaconic Acid Polyester Grafting. *ACS Applied Polymer Materials* **2025**, *7* (7), 4371−4382.
(34) Spanu, C.; Locatelli, E.; Sambri, L.; Comes Franchini, M.; Maturi, M. Photocurable Itaconic Acid-Functionalized Star Polycaprolactone in Biobased Formulations for Vat Photopolymerization. *ACS Applied Polymer Materials* **2024**, *6* (4), 2417−2424.
(35) Lim, J.; Ahn, Y.; Cho, H.; Kim, J. Optimal strategy to sort plastic waste considering economic feasibility to increase recycling efficiency. *Process Safety and Environmental Protection* **2022**, *165*, 420−430.
(36) Lange, J.-P. Managing Plastic Waste—Sorting, Recycling, Disposal, and Product Redesign. *ACS Sustainable Chem. Eng.* **2021**, *9* (47), 15722−15738.
(37) Prasanna Kar, G.; Lin, X.; Terentjev, E. M. Fused Filament Fabrication of a Dynamically Crosslinked Network Derived from Commodity Thermoplastics. *ACS Applied Polymer Materials* **2022**, *4* (6), 4364−4372.
(38) Crapnell, R. D.; Sigley, E.; Williams, R. J.; Brine, T.; Garcia-Miranda Ferrari, A.; Kalinke, C.; Janegitz, B. C.; Bonacin, J. A.; Banks, C. E. Circular Economy Electrochemistry: Recycling Old Mixed Material Additively Manufactured Sensors into New Electroanalytical

Sensing Platforms. *ACS Sustainable Chem. Eng.* **2023**, *11* (24), 9183–9193.
(39) Mohammed, M. I.; Wilson, D.; Gomez-Kervin, E.; Tang, B.; Wang, J. Investigation of Closed-Loop Manufacturing with Acrylonitrile Butadiene Styrene over Multiple Generations Using Additive Manufacturing. *ACS Sustainable Chem. Eng.* **2019**, *7* (16), 13955–13969.
(40) Zander, N. E. Recycled Polymer Feedstocks for Material Extrusion Additive Manufacturing. In *Polymer-Based Additive Manufacturing: Recent Developments*; ACS Symposium Series, Vol. *1315*; American Chemical Society, 2019; pp 37–51.
(41) Oladapo, B. I.; Bowoto, O. K.; Adebiyi, V. A.; Ikumapayi, O. M. Net zero on 3D printing filament recycling: A sustainable analysis. *Science of The Total Environment* **2023**, *894*, 165046.
(42) Giani, N.; Mazzocchetti, L.; Benelli, T.; Picchioni, F.; Giorgini, L. Towards sustainability in 3D printing of thermoplastic composites: Evaluation of recycled carbon fibers as reinforcing agent for FDM filament production and 3D printing. *Composites Part A: Applied Science and Manufacturing* **2022**, *159*, 107002.
(43) Mamatha, S.; Biswas, P.; Johnson, R. Digital light processing of ceramics: an overview on process, materials and challenges. *Progress in Additive Manufacturing* **2023**, *8* (5), 1083–1102.
(44) Ligon-Auer, S. C.; Schwentenwein, M.; Gorsche, C.; Stampfl, J.; Liska, R. Toughening of photo-curable polymer networks: a review. *Polym. Chem.* **2016**, *7* (2), 257–286.
(45) Zhang, B.; Kowsari, K.; Serjouei, A.; Dunn, M. L.; Ge, Q. Reprocessable thermosets for sustainable three-dimensional printing. *Nat. Commun.* **2018**, *9* (1), 1831.
(46) Kloxin, C. J.; Scott, T. F.; Adzima, B. J.; Bowman, C. N. Covalent Adaptable Networks (CANs): A Unique Paradigm in Cross-Linked Polymers. *Macromolecules* **2010**, *43* (6), 2643–2653.
(47) Chen, J.; Li, L.; Luo, J.; Meng, L.; Zhao, X.; Song, S.; Demchuk, Z.; Li, P.; He, Y.; Sokolov, A. P.; et al. Covalent adaptable polymer networks with CO2-facilitated recyclability. *Nat. Commun.* **2024**, *15* (1), 6605.
(48) Kloxin, C. J.; Bowman, C. N. Covalent adaptable networks: smart, reconfigurable and responsive network systems. *Chem. Soc. Rev.* **2013**, *42* (17), 7161–7173.
(49) Yue, L.; Su, Y.-L.; Li, M.; Yu, L.; Montgomery, S. M.; Sun, X.; Finn, M. G.; Gutekunst, W. R.; Ramprasad, R.; Qi, H. J. One-Pot Synthesis of Depolymerizable δ-Lactone Based Vitrimers. *Adv. Mater.* **2023**, *35* (29), 2300954.
(50) Yue, L.; Su, Y.-L.; Li, M.; Yu, L.; Sun, X.; Cho, J.; Brettmann, B.; Gutekunst, W. R.; Ramprasad, R.; Qi, H. J. Chemical Circularity in 3D Printing with Biobased Δ-Valerolactone. *Adv. Mater.* **2024**, *36* (34), 2310040.
(51) Carmenini, R.; Sanz de León, A.; Benelli, T.; Giorgini, L.; Comes Franchini, M.; Molina, S. I.; Maturi, M. One-pot depolymerization-repolymerization of PET waste into sustainable photocurable liquid copolyesters for high-performance additive manufacturing. *Green Chem.* **2025**, *27* (40), 12830–12843.
(52) Kolibaba, T. J.; Killgore, J. P.; Caplins, B. W.; Higgins, C. I.; Arp, U.; Miller, C. C.; Poster, D. L.; Zong, Y.; Broce, S.; Wang, T.; et al. Results of an interlaboratory study on the working curve in vat photopolymerization. *Additive Manufacturing* **2024**, *84*, 104082.
(53) Li, X.-R.; Wang, X.-L.; Koseki, H. Study on thermal decomposition characteristics of AIBN. *Journal of Hazardous Materials* **2008**, *159* (1), 13–18.
(54) Seok, W.; Jeon, E.; Kim, Y. Effects of Annealing for Strength Enhancement of FDM 3D-Printed ABS Reinforced with Recycled Carbon Fiber. *Polymers* **2023**, *15*, 3110.
(55) Zhao, J.; Guo, C.; Zuo, X.; Román, A. J.; Nie, Y.; Su, D.-X.; Turng, L.-S.; Osswald, T. A.; Cheng, G.; Chen, W. Effective mechanical properties of injection-molded short fiber reinforced PEEK composites using periodic homogenization. *Advanced Composites and Hybrid Materials* **2022**, *5* (4), 2964–2976.
(56) Halpin, J. C. Stiffness and Expansion Estimates for Oriented Short Fiber Composites. *Journal of Composite Materials* **1969**, *3* (4), 732–734.
(57) Affdl, J. C. H.; Kardos, J. L. The Halpin-Tsai equations: A review. *Polym. Eng. Sci.* **1976**, *16* (5), 344–352.
(58) Gholami, F.; Pakzad, L.; Behzadfar, E. Morphological, interfacial and rheological properties in multilayer polymers: A review. *Polymer* **2020**, *208*, 122950.
(59) Zhang, X.; Xu, Y.; Zhang, X.; Wu, H.; Shen, J.; Chen, R.; Xiong, Y.; Li, J.; Guo, S. Progress on the layer-by-layer assembly of multilayered polymer composites: Strategy, structural control and applications. *Prog. Polym. Sci.* **2019**, *89*, 76–107.
(60) Chen, C. P.; Lakes, R. S. Analysis of high-loss viscoelastic composites. *J. Mater. Sci.* **1993**, *28* (16), 4299–4304.
(61) Cai, Y.; An, X.; Zou, Q.; Fu, H.; Yang, X.; Zhang, H. Mechanical properties and failure mechanisms of composite laminates with classical fabric stacking patterns. *J. Mater. Sci.* **2021**, *56* (20), 11814–11827.
(62) Sharma, N. K.; Mehra, D. Review of Optimized Technologies for Cryogenic Grinding. *INTERNATIONAL JOURNAL OF ENGINEERING RESEARCH & TECHNOLOGY (IJERT)* **2014**, *2* (3), 1.
(63) Rizvi, S. F. J.; Miran, S.; Azam, M.; Arif, W.; Wasif, M.; Garcia, H. P. Numerical Analysis of a Liquid Nitrogen (LN2) Engine for Efficient Energy Conversion. *ACS Omega* **2021**, *6* (24), 15663–15673.
(64) Bhagwat, S. S.; Li, Y.; Cortés-Peña, Y. R.; Brace, E. C.; Martin, T. A.; Zhao, H.; Guest, J. S. Sustainable Production of Acrylic Acid via 3-Hydroxypropionic Acid from Lignocellulosic Biomass. *ACS Sustainable Chem. Eng.* **2021**, *9* (49), 16659–16669.
(65) Maturi, M.; Locatelli, E.; Sanz de Leon, A.; Comes Franchini, M.; Molina, S. I. Sustainable approaches in vat photopolymerization: advancements, limitations, and future opportunities. *Green Chem.* **2025**, *27* (29), 8710–8754.